Recent progresses in the inspection of aerospace components by infrared thermography

by Clemente Ibarra-Castanedo*, Ermanno Grinzato**, Sergio Marinetti**, Paolo Bison**, Marc Genest[+], Marc Grenier*, Jean-Marc Piau*, Abdelhakim Bendada* and Xavier Maldague*

*Computer Vision and Systems Laboratory, Department of Electrical and Computer Engineering, Université Laval, Quebec City, Canada G1K 7P4, Phone: +1(418) 656-2962, Fax: +1(418) 656-3594, E-mail: {IbarraC, Bendada, MaldagX}@gel.ulaval.ca, {Marc.Grenier.3, Jean-Marc.Piau.1}@ulaval.ca

**Istituto per le Tecnologie della Costruzione - Consiglio Nazionale delle Ricerche (ITC-CNR), Corso Stati Uniti, 4-35127, Padova, Italy. Phone: +39(049)829-5722, Fax: +39(049)829-5728, E-mail: {Ermanno.Grinzato, Sergio.Marinetti,Paolo.Bison}@itc.cnr.it

[+]Institute for Aerospace Research (IAR), National Research Council Canada (NRC), 1200 Montreal Road, Bldg. M-14, Room 130, Ottawa, ON, Canada, K1A 0R6, E-mail: Marc.Genest@nrc-cnrc.gc.ca.

Abstract

The use NonDestructive Testing and Evaluation (NDT&E) techniques for the inspection of aerospace materials has progressively increase in the last few decades as commercial and military aircrafts exceed their initial design life. Aerospace components are typically made of aluminium, honeycomb structures, composites or fibre metal laminates (FML), which are affected by different types of anomalies, namely: delaminations, disbonds, water ingress, node failure and core crushing. Possible causes are either material contamination introduced during manufacture, *e.g.* dirt, solvents, moisture, oils, etc.; or by damages caused during in-flight operation, *e.g.* after impact. Infrared thermography techniques have proven to be an effective way to detect and, in many cases, to quantify the degree of surface and subsurface damage on such components. Several configurations have been proposed to achieve an active thermography inspection ranging from *passive* inspection, *i.e.* without applying any external stimulation, to *active* approaches, in which an external source of energy is used to produce a thermal contrast between the non-defective and the defective material. The thermal stimulation can be delivered to the specimen surface by optical, mechanical, electromagnetic or other means. The physics and the practical considerations behind these approaches are different in all cases, and the selection of one or another will depend on the specific application and the availability of the equipment. In this paper, a review of recent developments on the thermographic inspection of aerospace materials is proposed. Some guidelines, supported with examples on real and academic specimens, are provided to illustrate the most suitable technique to be considered for some conventional applications.

Keywords: infrared thermography, fibre metal laminates, honeycomb structures, composites, aluminium.

1. 1. Introduction

Infrared thermography is a nondestructive testing and evaluation (NDT&E) technique allowing fast inspection of large surfaces [1]. There are two **approaches** to infrared thermography: (1) *passive*, in which the features of interest are naturally at a higher or lower temperature than the background (e.g. surveillance, medical and biological applications); and (2) *active*, which requires an external energy source to produce a thermal contrast between the feature of interest and the background.

Practically *any* energy source can be used for stimulation, from cold or hot air to water jets, or frequency and amplitude modulated acoustic waves [2]. **Excitation forms** can be divided in four types [3]: *optical*, *mechanical*, *electromagnetic* or other. Optical energy is normally delivered *externally*, *i.e.* heat is produced at the surface of the specimen and then travels through the specimen to the subsurface anomaly (defect) and back to the surface. Mechanical energy on the other hand, can be considered as an *internal* way of stimulation, since heat is generated at the defect interface and then travels to the surface. In electromagnetic excitation, Eddy currents are *externally* induced to the material (electro-conductor), and heat is produced *internally* from the circulation of these currents in the material. There are also different **techniques** depending on the stimulation source, basically: *pulsed* or *modulated*. *Step heating* is also found in literature, referring to a long pulse excitation, and *line excitation* can be employed as well, *i.e.* the camera and excitation source moving while the specimen remains static or vice versa [1]. Finally, there are two **configurations** in which an active thermography inspection can be performed, it can be done in *reflection* mode, *i.e.* excitation and data acquisition are carried out on the same side, or in *transmission*, i.e. the specimen is stimulated from one side whilst data is recorded on the opposite side. Usually in aerospace, there is no direct access to both sides of the component. Hence, the reflexion mode is often used.

The final decision on the most appropriate approach, excitation form, technique and configuration to be used is made depending on the application. For instance, active thermography is the most suitable approach for aerospace NDT&E since aircraft parts are normally at thermal equilibrium during the inspection. Pulsed thermography using optical excitation (flashes) in reflexion mode is often privileged for the inspection of

aerospace components *in situ*. Nevertheless, the passive approach can also be considered for aircraft inspection, for instance, right after landing when thermal contrast between the structure and the internal defects, *e.g.* water ingress, is very large. Mechanical excitation provides excellent results in some situations for which other stimulation forms do not provide suitable results, such as detection of surface micro-cracks using ultrasound stimulation [4]. Electromagnetic stimulation is relatively new on the field, although it has already shown a great potential on the development of portable equipment with results comparable to optical and mechanical stimulations for some defect types. Furthermore, in at least one study, it was found that node failure at the core of honeycomb structures was detected only using inductive excitation [5].

A specific nomenclature is adopted depending on the energy source. For instance, pulsed thermography (PT) and lock-in (or modulated) thermography (LT) are generally used when working with optical stimulation [2]. Data obtained by optical stimulation, in either PT or LT, is processed by the fast Fourier transform (FFT), which is commonly refer as pulsed phase thermography (PPT) [6], [7] in the case of pulsed thermographic data; and phase angle thermography [8] or phase sensitive thermography [9] in the case of modulated data. Results are presented in the form of *phasegrams*, *i.e.* a map of the specimen surface indicating the phase delay of the output signal with respect to the input. There are many other advanced processing techniques developed to improve the PT transient signal [10]. Thermographic signal reconstruction (TSR) [11] is one of such techniques. It allows reducing the amount of data, to de-noise the signal and to further process synthetic data using first and second time derivative images as well as the FFT, which considerably improve the signal-to-noise ratio. Space being limited and bibliography being abundant on the matter, interested readers can refer to the provided references for more details. In the case of mechanical stimulation, the terms thermosonics [12], ultrasound thermography [13] or vibrothermography [4] are adopted in either *burst* [14], *i.e.* pulsed; and frequency modulated or frequency/amplitude modulated configurations [15]. Vibrothermography (VT), either burst or modulated, requires much more attention to experimental parameters than the pulsed configuration [16], [17]: the pressure applied between the horn and the specimen, the contact area between the horn and the specimen and the duration of the stimulation have a great impact on the thermal response. The longer the transducer operates at the surface; the most heat is released at the contact surface, increasing the probability of damaging the area. Usually, when all these experimental factors are correctly addressed, raw thermograms present adequate contrast to detect defects. A simple cold image subtraction may help as well to improve contrast or the FFT algorithm can be used to process VT data when required. Finally, electromagnetic excitation is achieved by inducing Eddy currents through electromagnetic coils and it is commonly referred as thermo-inductive thermography [18], induction thermography [19] or Eddy current thermography (ECT) [20]. As is the case for optical and ultrasound excitation, both pulsed [21] and lock-in [22] configurations can be used. Another possible active thermography configuration is line excitation, *i.e.* the specimen is fixed while the camera moves behind the source at a controlled speed. No temporal signal processing is performed in this case. Images are reconstructed by retrieving the maximum thermal contrast for every pixel.

In this study, two common aerospace materials, honeycomb and GLARE, were tested by means of optical, mechanical and electromagnetic stimulation. The experimental results presented herein, allowed deriving some conclusions about the most suitable energy source for each particular case.

2. Inspection of honeycomb structures

2.1. Sandwich panel

Sandwiched structures made of a honeycomb core between two multi-layer carbon fibre reinforced plastic (CFRP) facesheets are very common in aerospace parts. This kind of structure is normally affected by anomalies such as delaminations (between plies in the facesheet), disbonds (between the inner facesheet and the core), water ingress, and core crushing. Possible causes for a delamination are either material contamination, *e.g.* dirt, solvents, moisture, oils, etc., introduced during manufacture or damage caused by in-flight operation. Core crush might occur after impact.

A sandwiched panel, shown in Figure 1, was designed to simulate the most common defect types listed above. The panel consists of an aluminium honeycomb core of 1.6 cm between two 10-ply CFRP. The specimen is divided into five zones as depicted in Figure 1a. A photograph of the specimen, taken during vibrothermography inspection, is shown in Figure 1b. In Zone I, twenty (20) Teflon® inserts of different dimensions and thicknesses are placed between CFRP plies at different locations and depths as specified in Table 1 to simulate delaminations between plies. In Zone II, six Teflon® inserts of different dimensions were inserted between the adhesive and the core (top row) and between the facesheet and the adhesive (bottom row), simulating skin to core disbonds at those locations. In Zone III, twelve cells were filled with water to simulate water ingress into the core. Water was injected into the cells through small wholes perforated in the opposite face of the panel to avoid damaging the panel side facing the camera (to which the optical stimulation was directed). Zone IV contains two impacts at 4 J (left) and 6 J (right), which are intended to simulate real collisions. Lastly, Zone V contains three honeycomb core node failure regions covering 3, 5 and 10 nodes as indicated.

Zone I was first inspected using optical excitation using pulsed and lock-in techniques. It is possible to detect almost all of the defects from the PPT and LT phasegrams in Figure 2a and b, respectively, with the exception of defect #10, which has a size-to-depth ratio very close to unity (D/z_{10}=1.2), see Table 1. Defect #18

has also a small size-to-depth ratio (D/z_{10} = 1.5). However, defect #18 is thicker than defect #10 (t_{10} = 0.16 mm *vs.* t_{18} = 0.33 mm). Therefore, it can be concluded that defect detectability by optical stimulation is affected not only by the defect size-to-depth ratio, but also by its thickness. The empirical rule of thumb of detectability D/z~2 constitutes a useful guideline [2].

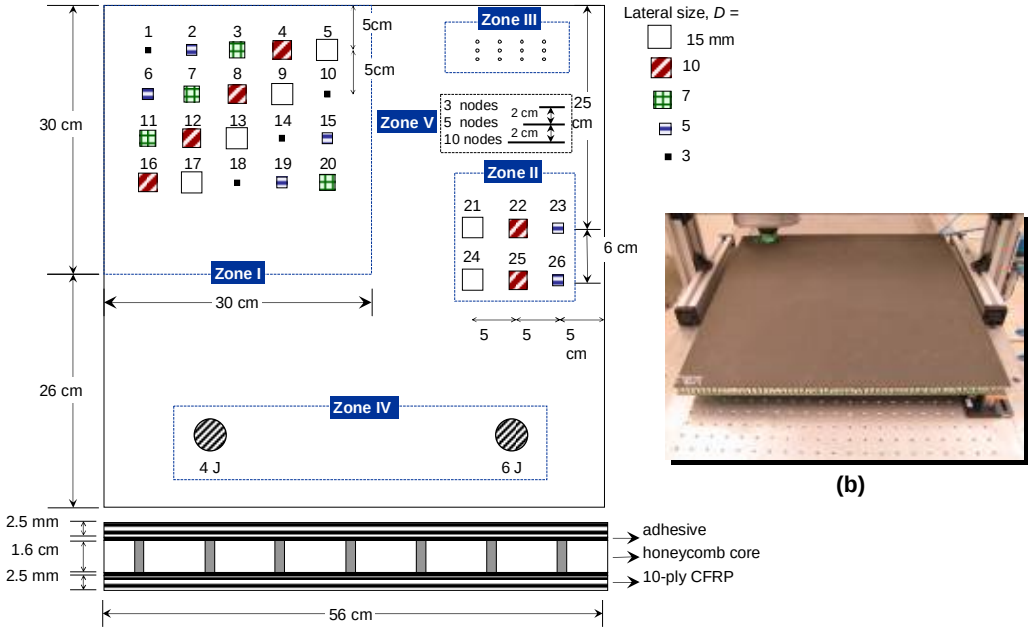

Figure 1. (a) Geometry and defect distribution of the honeycomb specimen, (b) specimen photograph during vibrothermography inspection.

Table 1. Teflon® inserts distribution for Zone I and Zone II.

	Defect number	Thickness, *t* [mm]	Lateral size, *D* [mm]	Between plies	Depth, *z* [mm]	Ratio *D/z*
Zone I	1	0.16	3	1 and 2	0.25	12
	2	0.16	5	2 and 3	0.5	10
	3	0.16	7	3 and 4	0.75	9.3
	4	0.16	10	4 and 5	1	10
	5	0.16	15	5 and 6	1.25	12
	6	0.16	5	6 and 7	1.5	3.3
	7	0.16	7	7 and 8	1.75	4
	8	0.16	10	8 and 9	2	5
	9	0.16	15	9 and 10	2.25	6.7
	10	0.16	3	9 and 10	2.25	1.3
	11	0.33	7	1 and 2	0.25	28
	12	0.33	10	2 and 3	0.5	20
	13	0.33	15	3 and 4	0.75	20
	14	0.33	3	4 and 5	1	3
	15	0.33	5	5 and 6	1.25	4
	16	0.33	10	6 and 7	1.5	6.7
	17	0.33	15	7 and 8	1.75	8.6
	18	0.33	3	8 and 9	2	1.5
	19	0.33	5	9 and 10	2.25	2.2
	20	0.33	7	9 and 10	2.25	3.1
Zone II	21	0.16	15	adhesive and core	2.5	6
	22	0.16	7	adhesive and core	2.5	2.8
	23	0.16	3	adhesive and core	2.5	1.2
	24	0.16	15	face sheet and adhesive	2.5	6
	25	0.16	7	face sheet and adhesive	2.5	2.8
	26	0.16	3	face sheet and adhesive	2.5	1.2

Although PPT phasegrams show better contrast for some inserts (defects #1 to 5 and #11 to 17), the LT phasegram provide a better overall detection, being able to detect all defects from a single phasegram. This is a logical result since several hundred images at a single frequency where used to obtain the LT phasegram contrary to PPT, for which a large number of phasegram at different frequencies are obtained by processing a 2 times larger thermogram sequence, see [7] for details on PPT processing.

Ultrasonic excitation was also used. As seen in Figure 2c, lock-in vibrothermography was able to detect 6 of the 10 inserts having a thickness *t*=0.33 mm, whilst a weak signature can be noticed for only a few of them having *t*=0.16 mm. Ultrasound waves travel through the specimen until they reach an air gap in the interface between the insert and the material, which allows the defect to vibrate generating heat locally. If little or no air is present, the heat signature would be weak at this location. Apparently, the thicker inserts are more likely to produce larger deformations than thinner inserts between plies, trapping air as a consequence. Hence, the preferred dissipation path for ultrasounds would be at these locations. Real delaminations however will behave differently. For instance, Figure 7 presents some results for delaminations simulated using different kinds of inserts. Results from ECT are shown in Figure 2d. This image is the result of a reconstruction of three line inspections to cover the whole area (Zone I). No processing was carried out in this case. The image reconstruction process consisted of retrieving the maximum thermal contrast value for each pixel, which usually corresponds to the first available value after stimulation, and constructing a single image, *i.e.* a *maxigram*. At least 11 of the 20 inserts can be clearly seen (defects #3, 4, 5, 8, 9, 11, 12, 13, 15, 16, 17 and 20), however with lower contrast than optical stimulation results. The presence of other 4 defects can also be inferred (defects #2, 7, and 19). These results are encouraging. More tests need to be run (using higher excitation frequencies for example) to improve defect detection.

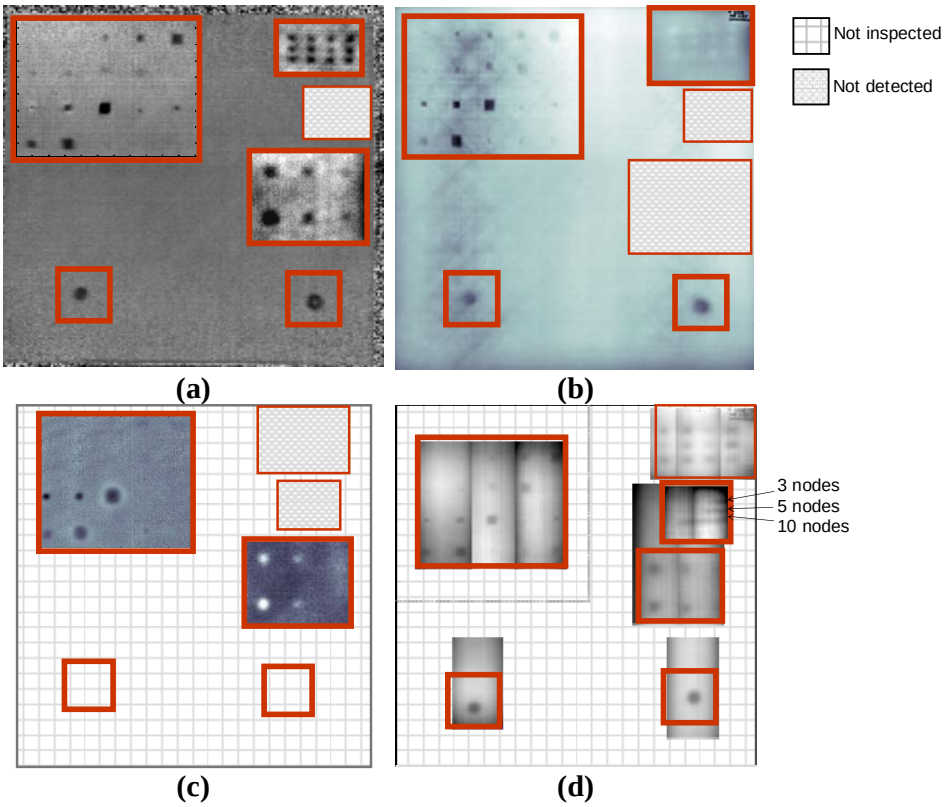

Figure 2. Honeycomb specimen, Zone IV (impact damage) and Zone V (cut honeycomb cells): (a) synthetic PPT phase at f = 0.8 Hz, (b) LT phase at f = 0.002 Hz, and (c) composed maximum contrast thermogram from line inspection by ECT.

In Zone II, all the inserts have a thickness of *t* = 0.16 mm, see Table 1. PT results processed by TSR clearly show the six inserts. On the other hand, both VT and ECT show only the four largest defects, with VT results having better defect contrast. It should be noted however that a 640x512 FPA camera was used for VT inspection whilst a 160x128 microbolometer camera was used in the case of ECT. Water ingress in Zone III was successfully detected by optical PT, optical LT, and line inspection ECT (Figure 2a, b and d), although only a weak signature can be detected in the latter two. Water ingress was not examined by VT. Impact damages in Zone IV, at 4 and 6 J, are clearly seen in all cases. It is interesting to note that defects in Zone V, *i.e.* honeycomb core node failure, were detected only by ECT, even though the signal is relatively weak. It appears that electromagnetic stimulation is well fitted for the inspection of this type of defects since Eddy currents propagate at their vicinity generating heat at these locations. Optical excitation on the other hand, is not very effective in this case given that heat is generated at the surface from where it travels through the specimen in all directions. Suitable results by VT for Zone IV and Zone V were not available at this point.

2.2. Honeycomb aircraft door

Figure 3 shows a GFRP door with a honeycomb core developed for Airbus by SABCA Limburg N. V. (Société Anonime Belge de Constructions Aéronautiques). The specimen's front surface was painted in black, as seen in Figure 3a, and inspected by pulsed thermography.

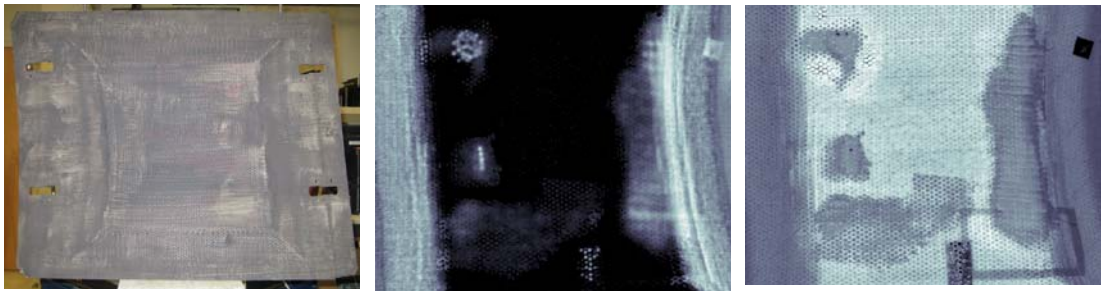

(a) **(b)** **(c)**

Figure 3. Airbus door specimen: (a) front view of the panel with the surface painted in black, (b) PPT phasegram at f= 0.04 Hz, and (c) PPT phasegram at f= 0.45 Hz.

Figure 3b and c present the PPT phase results at two frequencies. At low frequencies (*f*= 0.04 Hz, see Figure 3b) deep features are detected (inserted material used to simulate water ingress); whilst at higher frequencies (*f*= 0.45 Hz, see (Figure 3c), it is possible to see features that are at or very near the surface. It is possible to detect all four repair zones and other surface features such as adhesive tape, adhesive tape residues, brush trail marks (left during the application of water-based black painting) and a square mark on the bottom right corner from the phasegram in Figure 3c.

This example demonstrates the capabilities of the three techniques (DAC, TSR and PPT) for *qualitatively* detecting and analysing surface and subsurface defects in aerospace components. However, it is also important to carry out *quantitative* analysis in many cases. The next paragraph explains how TSR and PPT can be combined to estimate the depth of internal defects.

2.3. Depth quantification in CF-18 rudders

Flight control surfaces of CF-18 aircraft, such as rudders, are another example of aerospace structure made of honeycomb sandwich material. A front side photograph of a rudder portion used for the PT experiments is shown in Figure 4a.

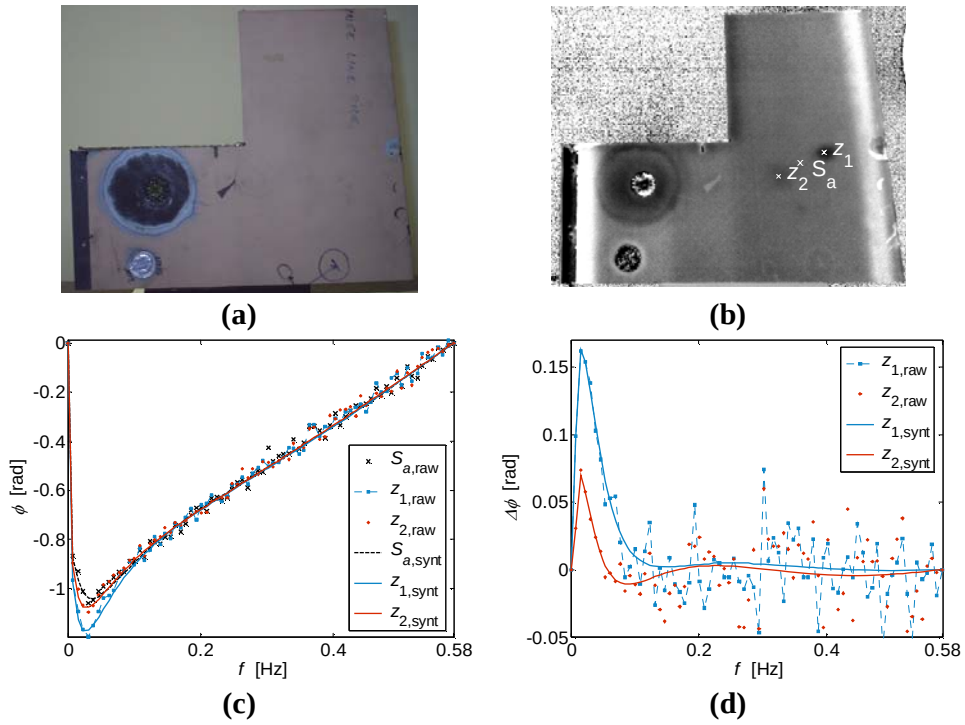

Figure 4. Rudder specimen: (a) Front (left column) and back (right column) side photographs, and synthetic corresponding phasegrams (from a 9th degree TSR polynomial fitting) at f= (b) 0.02, (c) 0.04, and (d) 0.2 Hz (Δt=860 ms, w(t)= 129 s, N=150).

A phasegram showing the defective and reference (Sound area, S_a) areas is presented in Figure 4b. Phase and phase contrast profiles are shown in Figure 4c and d, respectively. Given the considerably high noise levels affecting phase data, PPT was applied to a synthetic sequence obtained by TSR in order to detect the blind frequency f_b. This has an effective filtering effect on thermal data, which as seen produces de-noised phase profiles. The data filtering effect of applying the PPT algorithm to TSR synthetic data becomes more evident when analyzing the phase contrast profiles in Figure 4d. The PPT phase from raw thermal data is also included in these graphs to provide an indication of the levels of noise. The calculated blind frequencies allowed determining the depth of both defects: z_1=0.5 mm and z_2=2 mm. From these results it can be concluded that, defect number 1 is more likely due to an impact damage in the CFRP plies, while defect number 2 is deeper, corresponding possibly to a honeycomb crashed core. These observations were corroborated by visual (human) inspection.

3. Inspection of GLARE samples

GLARE is a hybrid material from the family of the fibre metal laminates (FML), which consist of alternating layers of thin metal (*e.g.* aluminium) sheets (0.3–0.5 mm thick) and glass fibre reinforced prepregs (0.25–0.5 mm thick). This configuration provides very good fatigue properties, good impact, damage tolerance and fire resistance characteristics. Three sets of specimens having some of the most common defect types found in GLARE were fabricated to asses the potential use of active thermography.

First, a set of GLARE specimens were prepared for impact damage testing using a falling weight impact. A lead-filled tube with a standard hemispherical 8 mm diameter steel ball was used as the impacter. A sliding plate at the base of the guiding tower allows the impacter tube to be caught after impact to prevent secondary impacts of the sample. The impact energy was calculated using the standard equation: $E = mgh$, where: m is the mass of the impacter, g is the acceleration due to gravity (9.81 m/s) and h is the height from which the weigh was dropped. Only pulsed thermography results are available at this point. Results for two of the specimens are presented in Figure 5. It was possible to view the impact damage on the surface, especially in the case of the thinner composite panels such as specimen GLARE006 (Figure 5, top). Furthermore, even in the case of the thicker samples as specimen GLARE007 (Figure 5, bottom) the damage areas, created by the impact damage testing, could be picked up by pulsed thermography as can be seen in Figure 5a. In accordance with the phase probing properties [7], the phasegrams at 1 Hz (Figure 5b) provide information about deeper features than the phasegrams at 0.15 Hz. It can be observed from these results that the extent of damage is greater, for the case of a thin plate subjected to a high energy impact (8 J), than for a thick plate subjected to a lower impact energy (4 J), as expected.

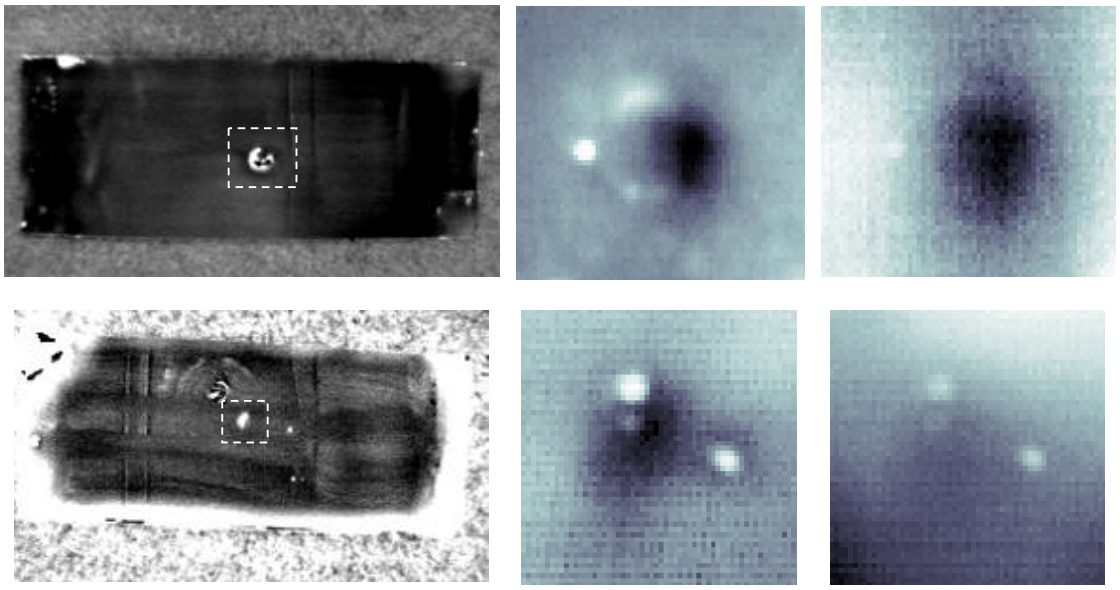

(a) **(b)** **(c)**

Figure 5. Results for specimens GLARE006 (top) and GLARE007 (bottom) after impact damage testing using 8 and 4 J, respectively: (a) thermogram, and the corresponding phasegrams of the cropped portion obtained by PPT at f =(b) 1 and (c) 0.15 Hz.

C-scan ultrasound is routinely used in the assessment of GLARE panels. However, the inspection is lengthy and affected by the shape of the part with the component being removed from the aircraft as shown in Figure 6. Pulsed thermography results (Figure 6, bottom) demonstrate that it is possible to detect the lack of material down to a certain depth. Only two of the three artificial defects can be seen in either front or back side testing. Although experimental results by ECT are not available at this point, the conventional Eddy current results

show perfectly the three defects, which let us to believe that Eddy current thermography could provide comparable results with a fully portable equipment for *in situ* inspections.

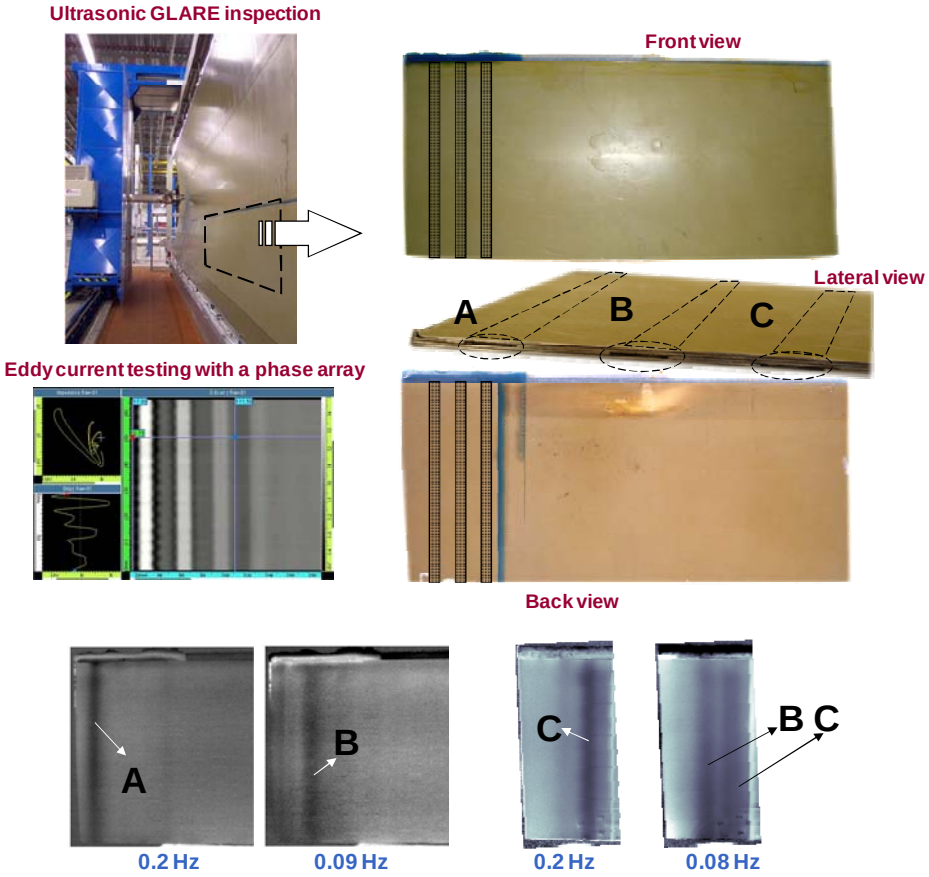

Figure 6. GLARE inspection by ultrasonic testing (top left), GLARE section with fabricated defects (right), and results on the GLARE section by phase array Eddy current testing (bottom left).

Finally, a GLARE specimen (Al/0°/90°/0°/Al/0°/90°/0°/Al/0°/90°/0°/Al, using unidirectional glass-fibre epoxy layer FM94S2) was fabricated with simulated delamination of four kinds: 1-ply release film, 2-plies release film, Kapton®/Frekote® inserts and aluminium shim/Frekote® inserts. All defects can be seen by pulsed thermography (Figure 7a) with data processed by TSR, and most of them can be detected by VT (Figure 7b), which confirms the likelihood of detecting delamination in GLARE structures. Surface features are also seen in the PT result as highlighted by the dotted circle in Figure 7a, which corresponds to a surface painting scraps having a very low emissivity. The VT result is less affected by surface artefacts as can be seen in Figure 7b, since subsurface heating is generated at the material-defect interface and not from the surface as in PT.

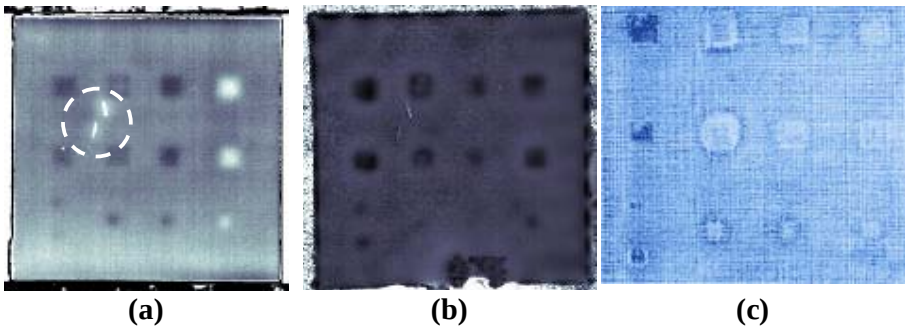

Figure 7. (a) first derivative image at t = 0.6 s, (b) vibrothermography result, and (c) C-scan ultrasounds (15 MHz).

Another interesting observation is that it is possible to differentiate between the inserted materials from the PT results. Aluminium inserts in particular have a distinctive signature with inverted sign as can be seen in the figure. An additional defect can be seen in the first column of defects (1-ply film release). This defect was not included in the specimen specifications from the manufacturer. C-scan results (Figure 7c) confirmed the existence of this defect.

4. Conclusions

Every material responds differently to thermal excitation depending on the way it has been stimulated. Thermography based on optical techniques, in general, provide very good defect resolution. However, results are strongly affected by surface features. Advanced signal/image processing is required to reduce their impact. For instance, PPT and TSR techniques allow detecting defects down to a depth of 2.5 mm, for defects having a size-to-depth ratio of approximately 2 and higher. Thermography using ultrasounds provide an interesting means for inspecting materials. It has the inconvenience of requiring a physical contact between the ultrasonic transducer and the specimen and that many experimental factors need to be addressed to obtain good results. Nevertheless, once all these factors are correctly addressed, inspection is extremely fast and results provide good defect contrast without processing. Cold image subtraction or the FFT can be used to improve contrast in some cases. Electromagnetic excitation is a relatively new field of investigation in active thermography. As in conventional Eddy current testing, ECT is limited to the inspection of conductor materials. When compared to optical or mechanical equipment it provides a more compact inspection configuration. Hence, commercial portable systems are starting to appear in the market.

REFERENCES

[1] Nondestructive Testing Handbook, Third Edition, Vol 3 Infrared and Thermal Testing, Chap 15, ASNT, 2001, p495-496.

[2] Maldague X. P. V. *Theory and Practice of Infrared Technology for NonDestructive Testing*, John Wiley-Interscience, 684 p., 2001.

[3] Ibarra-Castanedo C., Piau J-M., Guibert S., Maldague X. P. and Bendada A. "Chapter 14. Active infrared thermography techniques for the nondestructive testing of materials," in *Ultrasonic and Advanced Methods for Nondestructive Testing and Material Characterization*, C. H. Chen Ed., p 325-348, 2006.

[4] Piau J-M., Bendada A., Maldague X. P. and Legoux J-G. "Nondestructive inspection of open micro-cracks in thermallysprayed-coatings using ultrasound excited vibrothermography," *SPIE - The International Society for Optical Engineering, Thermosense XXIX*, Orlando, FL, April 9-13 2007, Eds. K. M. Knettel, V. Vavilov and J. J. Miles, **6541**:654112.

[5] Ibarra-Castanedo C., Grinzato E., Marinetti S., Bison P., Avdelidis N., Grenier M., Piau J-M., Bendada A. and Maldague X. P. "Quantitative assessment of aerospace materials by active thermography techniques," *Proc. QIRT 9 – Quantitative Infrared Thermography*, Krakow, Poland, July 2-5, 2008.

[6] Maldague X. P. and Marinetti S. "Pulse Phase Infrared Thermography," *J. Appl. Phys.*, **79**(5):2694-2698, 1996.

[7] Ibarra-Castanedo C. and Maldague X. "Pulsed Phase Thermography Reviewed," *QIRT J.*, **1**(1):47-70, 2004.

[8] Dillenz A., Zweschper T., Riegert G. and Busse G. "Progress in phase angle thermography," *Rev. Sci. Instrum.,* **74**(1):417-419, 2003.

[9] Busse G., Wu D. and Karpen W. "Thermal Wave Imaging with Phase Sensitive Modulated Thermography," *J. Appl. Phys.*, **71**(8):3962-3965, 1992.

[10] Ibarra-Castanedo C., Gonzalez D. A., Galmiche F., Bendada A. and Maldague X. P., "Recent Research Developments in Applied Physics On signal transforms applied to pulsed thermography" *Recent Research Developments in Applied Physics*, **9**:101-127 pages, 2006.

[11] Shepard S. M., Lhota J. R., Rubadeux B. A., Ahmed T., Wang D. "Enhancement and reconstruction of thermographic NDT data", *Proc. SPIE - The International Society for Optical Engineering, Thermosense XXIV*, Orlando, FL, 2002, Eds. X. P. Maldague and A. Rozlosnik, **4710**:531-535.

[12] Favro L. D., Han X., Ouyang Z., Sun G., Sui H. and Thomas R. L. "Infrared imaging of defects heated by a sonic pulse," *Rev. Sci. Instr*., 2000.

[13] Dillenz A., Zweschper T. and Busse G. "Progress in ultrasound phase thermography," *Proc. SPIE - The International Society for Optical Engineering, Thermosense XXVIII*, Orlando, FL, 2001, Eds. A. E. Rozlosnik and R. B. Dinwiddie, **4360**:574-579.

[14] Zweschper T., Riegert G. Dillenz A. and Busse G. "Ultrasound Burst Phase Thermography (UBP) for Applications in the Automotive Industry," *Rev. Quant. Nondestr. Eval.*, D. O. Thompson and D. E. Chimenti (eds.), **22**:531-536, 2003.

[15] Zweschper T., Riegert G., Dillenz A. and Busse G. "Frequency modulated elastic wave thermography," *Proc. SPIE - The International Society for Optical Engineering, Thermosense XXV*, Orlando, FL, 2003, Eds. K. E. Cramer and X. P. Maldague, **5073**:386-391.

[16] Shepard S. M., Ahmed T. and Lhota J. R. "Experimental considerations in vibrothermography," *Proc. SPIE - The International Society for Optical Engineering, Thermosense XXVI*, Orlando, FL, 2004, Eds. D. D. Burleigh, K. E. Cramer and G. R. Peacock, **5405**:332-335.

[17] Perez I. and Davis W. R. "Optimizing the thermosonic signal," in *Rev. Quant. Nondestr. Eval.*, D. O. Thompson and D. E. Chimenti (eds.), **22**:505-512, 2003.

[18] Oswald-Tranta B. "Thermo-inductive crack detection," *Nondestructive Testing and Evaluation*, vol. 22, 2007, pp. 137-153.

[19] Hillemeier B. "Location of Reinforcement by Induction-Thermography," *Proc. SPIE - The International Society for Optical Engineering, Thermosense VII,* Orlando, FL, 1984, Ed. A. G. Kantsios, **0520**:197-206.

[20] G. Zenzinger et al., "Thermographic crack detection by eddy current excitation," *Nondestructive Testing and Evaluation*, **22**:101-111, 2007.

[21] McCullough R. W. “Transient thermographic technique for NDI of aerospace composite structures,” *Proc. SPIE - The International Society for Optical Engineering, Thermosense XXVI,* Orlando, FL, Apr 13-15 2004*,* Ed. D. D. Burleigh, K. E. Cramer and G. R. Peacock, **5405**:390-402.

[22] Riegert G., Zweschper T., and Busse G. “Eddy-current lockin-thermography: Method and its potential,” *Journal de Physique IV*, vol. 125, Jun. 2005, pp. 587-591.